Astron. Astrophys. 354, 7–16 (2000)

ASTRONOMY AND ASTROPHYSICS

Radio imaging of core-dominated high redshift quasars

Peter D. Barthel[1], **Marianne Vestergaard**[2,3,4], **and Colin J. Lonsdale**[5]

[1] Kapteyn Astronomical Institute, P.O. Box 800, 9700 AV Groningen, The Netherlands
[2] NBIfAFG, Copenhagen University Observatory, Juliane Maries Vej 30, 2100 Copenhagen, Denmark
[3] Harvard-Smithsonian Center for Astrophysics, Cambridge, MA 02138, USA
[4] Department of Astronomy, The Ohio State University, 140 W. 18th Av., Columbus, OH 43210, USA (current address)
[5] MIT Haystack Observatory, Westford, MA 01886, USA

Received 16 July 1999 / Accepted 17 November 1999

Abstract. VLA imaging at kiloparsec-scale resolution of sixteen core-dominated radio-loud QSOs is presented. Many objects appear to display variable radio emission and their radio morphologies are significantly smaller than those of steep-spectrum quasars, consistent with these objects being observed at sight lines close to their (relativistic, $\gamma \approx 4$–7) jet axes. The usefulness of the radio source orientation indicator R_V, being defined as ratio of radio core and rest frame optical V-band luminosity, is confirmed.

Key words: galaxies: active – galaxies: jets – galaxies: quasars: general

1. Introduction: classes of radio-loud AGN

Radio-loud active galactic nuclei can to first order be classified as having either extended ($\gtrsim$ 15 kpc) or compact ($\lesssim$ 15 kpc) radio morphologies. The former class is characterized by steep, $\alpha \gtrsim 0.7$[1] radio spectra, signposting extended regions of optically thin synchrotron emission. Quasars or radio galaxies displaying prominent radio lobes – on size scales of tens to hundreds of kiloparsecs – invariably are characterized by steep radio spectra. The converse, however, is not true: compact morphologies are found in radio sources having flat as well as steep radio spectra. Compact steep-spectrum (CSS) radio sources are thought to be intrinsically small objects (e.g., Fanti et al. 1990), although some CSS objects may be small due to projection. Ultra-compact GPS (Gigahertz Peaked Spectrum) radio sources display inverted spectra longward and steep spectra shortward of the peak frequency (which usually occurs around 1 GHz) – see e.g., O'Dea (1998). It is likely that the classes of GPS, CSS, and extended steep-spectrum sources are connected through temporal evolution (e.g., Readhead et al. 1996, De Vries et al. 1998, O'Dea 1998).

Flat-spectrum radio sources invariably display a dominant compact flat-spectrum core component, but additional weak extended emission is usually present. In addition, VLBI imaging usually resolves the dominant core components into compact core-jet features, often displaying superluminal motion. Orr & Browne (1982) originally proposed that these core-dominated sources are simply extended, steep-spectrum objects viewed at small inclinations, relativistic flux boosting effects being responsible for the bright radio cores. Imaging observations of core-dominated quasars have yielded broad consistency with this model, as these objects usually display weak halo and/or (curved) jet emission of small angular extent (e.g., Kollgaard et al. 1990). Within unified models however, the parent population of the core-dominated quasars is not made up of lobe-dominated quasars, but of extended lobe-dominated radio galaxies (e.g., Urry & Padovani 1995). In these models, lobe-dominated quasars are thought to have jet inclination angles intermediate between the radio galaxies and the core-dominated quasars. Having data of a large, homogeneous sample of lobe-dominated steep-spectrum quasars at high redshift in hand (Lonsdale et al. 1993, LBM93 hereafter), we here present an investigation of this unification issue for high redshift quasars. The uniformity of the LBM93 data base coupled to new sensitive high resolution observations of core-dominated objects is expected to yield useful constraints on the relevant unification models.

2. Sample selection and VLA observations

2.1. Sample selection

In order to complement our LBM93 data base of steep-spectrum quasars, we selected a new sample of 16 powerful radio-loud quasars with spectral index criterion α_{408}^{5000} or $\alpha_{1400}^{5000} \lesssim 0.5$ at redshifts $z \sim 2$ to 3. We extracted these quasars from the Hewitt & Burbidge catalog (Hewitt & Burbidge 1993), using radio spectral data from the literature. Although our sample is not complete, having its size restricted by the observing time allocation, we are confident that it is representative of the population of powerful flat-spectrum radio-loud quasars at high redshift. Table 1 lists general information on the sample. Most of the radio spectral indices are in the range 0.3 – 0.5, while three objects with inverted spectral slope appear. Due to radio core variability at cm wavelengths – common in these objects – and

Send offprint requests to: Peter Barthel (pdb@astro.rug.nl)

[1] $S_\nu \propto \nu^{-\alpha}$

Table 1. The flat-spectrum quasar sample

Quasar[a]	Other name	RA(1950)	Dec(1950)	redshift	M_V	α_{1400}^{5000} [b]
0106+013	4C 01.02	01:06:04.55	+01:19:00.3	2.107	−27.3	0.31
0123+257	4C 25.05	01:23:57.28	+25:43:27.8	2.356	−28.2	−0.22
0206+293	B2	02:06:14.97	+29:18:34.7	2.195	−26.8	0.34
0226−038	4C −03.07	02:26:22.10	−03:50:58.3	2.066	−28.7	0.25
0317−023	4C −02.15	03:17:56.87	−02:19:26.2	2.092	−26.2	0.47
0458−020	4C −02.19	04:58:41.31	−02:03:33.9	2.286	−26.1	−0.48
0504+030	4C 03.10	05:04:59.24[c]	+03:03:57.7[c]	2.453	−26.9	0.54
1116+128	4C 12.39	11:16:20.82	+12:51:06.8	2.118	−26.4	0.27
1313+200	UT	13:13:58.64	+20:02:52.5	2.461	−27.4	0.29
1402−012	PKS	14:02:11.30	−01:16:02.5	2.522	−27.8	0.20
1442+101	OQ 172	14:42:50.58	+10:11:12.8	3.535	−28.4	0.54
1542+042	4C 04.53	15:42:29.75	+04:17:07.8	2.182	−27.6	0.35
1556−245	PKS	15:56:41.09	−24:34:11.0	2.818	−27.3	0.40[d]
1705+018	PKS	17:05:02.72	+01:52:37.5	2.577	−27.3	−0.27
2048+196	UT	20:48:56.58	+19:38:49.4	2.367	−27.2	0.24
2212−299	PKS	22:12:25.09	−29:59:20.0	2.706	−29.1	0.30[d]

[a] IAU convention
[b] $S_\nu \propto \nu^{-\alpha}$
[c] new measurement (see text)
[d] α_{2700}^{5000}

non-simultaneity of the measurements, the spectral index values will be mildly variable. On the basis of the information presented in Sect. 2.3 however it must be concluded that such variability would not affect our sample selection.

Optical QSO positions (B1950) were extracted from the literature or the Cambridge APM facility (http://www.ast.cam.ac.uk/∼apmcat/). One particularly inaccurate position, for 0504+030, was remeasured from a newly obtained R-band image of the QSO field, using APM star positions. Columns 3 and 4 of Table 1 list the optical QSO positions. Positional accuracies (3σ) for the optical QSOs are 1 arcsec, except for 0504+030 (1.″5). Absolute visual magnitudes were computed from the apparent magnitudes (Véron-Cetty & Véron 1987) using the cosmology[2] H_0=75 km s^{-1} Mpc^{-1}, q_0=0. In addition, these computations used optical continuum spectral index values $\alpha = 0.7$, and emission line corrections as specified in Véron-Cetty & Véron (1987 – their Fig. 2).

On the assumption of isotropic radiation, the inferred 5 GHz radio luminosities of these objects would be in the range $P_5 = 10^{27.4} - 10^{29.1}$ W Hz^{-1}. Due to anisotropy of the core radiation this assumption is most likely incorrect. As we will show below, the high luminosities in fact imply beamed, anisotropic radiation.

2.2. VLA imaging

The flat-spectrum quasar sample was observed with the NRAO Very Large Array, during two observing sessions: March 1990 and September 1995. All quasars were observed at 5 GHz (C-band), with the VLA in its high resolution A-array configuration, yielding a typical beam size of approximately 0.5 arcsec. Snapshot observations combining two scans of 2–5 minutes each, at different hour angles, were obtained in order to improve the shape of the synthesized beam.

Secondary phase and amplitude calibrators were observed before and after each scan. Primary calibrator was 3C 286, with appropriate baseline constraints, and adopted 5 GHz flux density as provided by the VLA staff: 7.379 Jy and 7.427 Jy, at IF1 and IF2, respectively. The calibration uncertainty is dominated by the uncertainty in the absolute flux density of the primary calibrator, which is a few percent. The array performed well: judged from the calibration sources, the antenna phase and amplitude calibration appeared stable to within a few percent.

The radio data were of high quality, and there was no need for extensive flagging of discrepant points. Reduction of the data was performed using standard NRAO AIPS image processing routines, including several steps of self-calibration (phase only, in a few cases followed by amplitude self-calibration). Several successive self-calibration and cleaning cycles generally led to a rapid convergence towards the maps presented here. Both full resolution maps, having synthesized beams between 0.35 and 0.60 arcsec, and tapered maps, having beams ∼1.2 arcsec were made. In the adopted cosmology, one arcsec corresponds to the range 8.7 – 9.2 kpc, for the redshifts under consideration.

2.3. Results and comments on individual sources

Several sources remain unresolved at the present kpc-scale resolution. Images of the resolved sources are shown in Figs. 3

[2] H_0=75, q_0=0 used throughout

Table 2. Quasar contour map specifications

Quasar	resolving VLA beam (maj.axis/min.axis/p.a.)	peak flux density (mJy/beam)	contour levels (mJy/beam)	Fig. no.
0106+013	0.67/0.42/-65°	1813	$1.0\times(-3,3,6,12,...,1536)$	3
0123+257	0.76/0.42/48°	1075	$1.4\times(-3,3,6,12,...,384)$	4
0226−038	0.45/0.37/2°	586	$0.5\times(-3,3,6,12,...,768)$	5
0317−023	0.41/0.39/-20°	159	$0.25\times(-3,3,6,12,...,384)$	6
0458−020	0.62/0.39/5°	3543	$1.5\times(-3,3,6,12,...,1536)$	7
0504+030	0.46/0.39/22°	332	$0.25\times(-3,3,6,12,...,768)$	8
1116+128	0.54/0.40/-85°	1673	$1.1\times(-3,3,6,12,...,768)$	9
1313+200	0.40/0.38/-51°	268	$0.6\times(-3,3,6,12,...,384)$	10
1542+042	0.49/0.43/-27°	457	$0.3\times(-3,3,6,12,...,768)$	11

Table 3. Quasar properties, measured/calculated from 5 GHz VLA data

Quasar	epoch (VLA obs.)	flux density (mJy)	extended flux density (mJy)	log(L_{total})[a] (W/Hz)	log($L_{ext.}$)[b] (W/Hz)	ang. size (arcsec)	lin. size (kpc)	log R_5^c	log R_V^d
0106+013	1990.2	1950	150	28.51	27.63	4.5	39.1	−0.08	3.68
0123+257	1990.2	1130	50	28.12	27.30	1.0	8.8	−0.05	3.22
0206+293	1990.2	280	–[e]	27.73			<1	0.00	3.15
0226−038	1990.2	650	70	27.98	27.28	3.5	30.3	−0.11	2.62
0317−023	1990.2	260	100	27.70	27.45	7.0	60.7	−0.41	3.08
0458−020	1990.2	3700	150	28.47	27.74	3.5	30.8	−0.05	4.55
0504+030	1990.2	480	160	28.19	27.85	4.0	35.5	−0.37	3.27
1116+128	1990.2	1800	100	28.46	27.46	2.7	23.5	−0.06	4.02
1313+200	1995.7	290	20	27.84	26.96	0.6	5.3	−0.08	2.99
1402−012	1995.7	340	–[e]	27.89			<1	0.00	2.97
1442+101	1990.2	1220	–[e]	29.05			<1	0.00	3.42
1542+042	1990.2	490	40	27.97	27.10	1.3	11.4	−0.09	3.00
1556−245	1995.7	380	–[e]	28.18			<1	0.00	3.31
1705+018	1995.7	570	–[e]	27.88			<1	0.00	3.43
2048+196	1995.7	110	–[e]	27.35			<1	0.00	2.63
2212−299	1995.7	410	–[e]	28.11			<1	0.00	2.61

[a] K-corrected using spectral index for integrated emission
[b] K-corrected adopting spectral index 0.80 for extended emission
[c] logarithm of fractional core flux density at 5 GHz emitted frequency, computed adopting spectral indices 0.80 and 0 for the extended and core emission respectively
[d] logarithm of ratio of radio core luminosity at 5 GHz emitted frequency to (K-corrected) optical V-band luminosity
[e] diffuse extended flux density up to about 20 mJy cannot be excluded – see text, Sect. 2.4

– 11, at the end of the paper. Typical (1σ) image noise levels are between 0.2 and 1 mJy/beam. Map parameters are listed in Table 2. All sources are individually described below. We will frequently compare our (epoch 1990.2 and 1995.7 – see Table 3) 5 GHz VLA flux densities with single dish values measured by Becker et al. (1991, B91 hereafter) in epoch 1987.8, and Griffith et al. (1995, G95 hereafter) in epoch 1990.9.

2.3.1. 0106+013

We measure a 5 GHz core flux density of 1.80 Jy and an additional flux density of 0.15 Jy in extended emission. Comparison with other measurements (B91: 3.47 Jy; G95: 2.08 Jy) indicates strong variability. The radio structure of 0106+013 is a 4.5 arcsec double, with a dominant core coincident with the optical QSO (Fig. 3). Our image is morphologically consistent with the 5 GHz VLA image of Kollgaard et al. (1990) and the lower resolution image of Murphy et al. (1993). The flux density contrast with the Kollgaard et al. data (core flux density 3.87 Jy, at observing epoch 1986.45) is nevertheless striking.

2.3.2. 0123+257

We measure a 5 GHz integrated flux density of 1.13 Jy, of which 1.08 Jy is in an unresolved nucleus and $\sim$0.05 Jy in extended emission, including an unresolved component, 1.0 arcsec SE of

the former (Fig. 4). Comparison with B91, measuring 1.33 Jy, indicates moderate 5 GHz variability.

2.3.3. 0206+293

This (B2) quasar is unresolved, hence the radio map is not shown. Our 5 GHz flux density of 0.28 Jy is consistent with the 1987 value (B91).

2.3.4. 0226−038

We measure a 5 GHz integrated flux density of 0.65 Jy, of which 0.58 Jy is in an unresolved nucleus and 0.07 Jy in additional components, straddling the former (Fig. 5). The overall angular size is 3.5 arcsec. As measured by Wall (1972), Parkes single dish data (0.55 Jy) are indicative of mild variability.

2.3.5. 0317−023

We detect a 5 GHz integrated flux density of 0.26 Jy, of which 0.16 Jy is in an unresolved nucleus and 0.10 Jy in additional components, towards the south and in a curved small scale jet towards the NE (Fig. 6). The overall angular size of 0317−023 is 7 arcsec. Neither the Green Bank single dish flux density (0.28 Jy – G95) nor the earlier Parkes figure (0.29 Jy – Wall 1972) are indicative of variability.

2.3.6. 0458−020

Well-known variable object at cm-mm wavelengths (e.g., Kühr et al. 1981, G95), and 'marginal' EGRET γ-ray source (Thompson et al. 1995). Our integrated 5 GHz flux density of $\sim$3.7 Jy implies a factor two of increase in comparison to earlier data (Kühr et al. 1981). A strong core (3.55 Jy at 5 GHz) is straddled by $\sim$0.15 Jy extended emission, yielding an overall angular size of $\sim$3.5 arcsec (Fig. 7). A tapered map demonstrates the reality of the faint emission NE of the nucleus. Our image is consistent with a MERLIN 408 MHz image (F. Briggs, priv. comm.; image also shown in Punsly 1995).

2.3.7. 0504+030

We detect a 5 GHz integrated flux density of 0.48 Jy, of which 0.32 Jy is in an unresolved nucleus and 0.16 Jy in a jet-hotspot structure towards the NW as well as faint emission towards the SE (Fig. 8). A tapered map demonstrates the reality of this 'counterjet' emission. The overall angular size of 0504+030 measures 4 arcsec. Our flux density determination is consistent with earlier ones (B91: 0.45 Jy, G95: 0.50 Jy), indicating little or no variability. In order to resolve a positional discrepancy for the optical QSO, we analyzed images of the field, taken using the 90cm ESO Dutch telescope on La Silla. Although the identification is secure now, we were unable to improve on the accuracy of the astrometry, due to the small number of suitable stars in the field of the QSO. We refer to Table 1 and the accompanying paragraph in Sect. 2.1.

2.3.8. 1116+128

Our measurements in comparison with literature data indicate fairly strong core variability. We detect 1.7 Jy in an unresolved core, and 0.1 Jy in a secondary component 2.7 arcsec towards the NW (Fig. 9). Our integrated 5 GHz flux density of 1.8 Jy is inconsistent with earlier values, which are in the range 1.3 – 1.6 Jy (Kühr et al. 1981). Our image is consistent with the lower resolution image of Murphy et al. (1993), although the latter shows some evidence for additional low surface brightness halo emission. O'Dea et al. (1988) also find evidence for diffuse emission, besides the unequal double morphology (having 1.5 Jy in the unresolved core).

2.3.9. 1313+200

This object originated in the University of Texas 365 MHz survey (Wills & Wills 1979). Our integrated 5 GHz flux density of 0.29 Jy – of which 0.27 Jy is in an unresolved component – is not indicative of strong variability by comparison with B91 (0.33 Jy). Our image shows an unresolved core and faint extended emission, 0.7 arcsec NNW (Fig. 10).

2.3.10. 1402−012

An unresolved source, having 5 GHz flux density 0.34 Jy. Wall (1972) reports a Parkes value of 0.81 Jy: the object must be strongly variable. Deconvolution gives evidence for small resolution effects in direction N-S. The radio map is not shown.

2.3.11. 1442+101

This is a well known GPS object, identified with the pre-1982 QSO redshift record holder OQ 172. The radio source is unresolved on the 0.1 arcsec scale, hence the radio map is not shown. VLBI observations on the other hand have revealed a highly bent core-jet structure on the milliarcsec scale (Udomprasert et al. 1997). Our flux density measurement of 1.22 Jy is consistent with earlier ones, e.g., Kühr et al. (1981), thereby indicating little or no variability.

2.3.12. 1542+042

We measure a 5 GHz core flux density of 0.45 Jy and an additional flux density of 0.04 Jy in extended emission. Most of this extended emission originates in a secondary component 1.3 arcsec E of the nuclear component (Fig. 11). There is evidence for additional low surface brightness halo emission both E and W of the nucleus, which is confirmed by a tapered image. Other measurements (B91: 0.41 Jy; G95: 0.54 Jy; Shimmins et al. 1975: 0.47 Jy) are indicative of a small level of variability.

2.3.13. 1556−245

We measure an unresolved 5 GHz flux density of 0.38 Jy; the radio map is not shown. Comparison with Parkes data (0.54 Jy – Bolton et al. 1975) indicates fairly strong variability.

2.3.14. 1705+018

We measure an unresolved 5 GHz flux density of 0.57 Jy; the radio map is not shown. Comparison with earlier data (e.g., Wall 1972: 0.58 Jy; B91: 0.42 Jy; G95: 0.46 Jy) yields evidence for moderate levels of variability.

2.3.15. 2048+196

We measure unresolved 5 GHz flux density of 0.11 Jy for this UT quasar, consistent with B91; the radio map is not shown.

2.3.16. 2212−299

We measure unresolved 5 GHz flux density of 0.41 Jy, consistent with the Parkes value (Wall et al. 1976); the radio map is not shown.

2.4. Source parameters

Measured parameters for the 16 quasars, as well as inferred quantities appear in Table 3. The flux densities were measured in various ways. Gaussian component fitting on the images was employed to determine the (unresolved) core flux densities. Flux density figures for the weak extended emission features were determined by adding the relevant CLEAN components in combination with examination of the short baseline amplitudes in the uv-plane. The estimated uncertainty in these figures (3σ) is 5–10 percent. Source intrinsic parameter computation used the adopted cosmology. We obviously do not list luminosities for undetected extended emission associated with unresolved objects. However, taking 20 mJy as a conservative flux density upper limit for such, probably diffuse low surface brightness emission, the relevant luminosity upper limit is $\sim 10^{27}$ W Hz^{-1} at the redshifts involved, which is a substantial value. The penultimate column in Table 3 specifies the radio core fraction at 5 GHz emitted frequency, $\log R_5$. These figures were computed from the entries in Columns 3 and 4, adopting canonical spectral index values of 0.80 and 0 for the extended and core emission, respectively. The final column lists values of the R_V parameter, introduced by Wills & Brotherton (1995), and defined as the ratio of the core radio luminosity at 5 GHz emitted frequency to the (K-corrected) optical V-band luminosity as computed from the absolute visual magnitudes. It is easy to show that $\log R_V = \log(L_{\rm core,5}) + M_V/2.5 - 13.7$. The next section will discuss this R_V parameter.

3. Discussion

Out of the sample of 16 core-dominated objects, nine objects display extended emission, generally morphologically asymmetric with respect to the dominant nuclear emission. This is entirely in agreement with earlier studies (e.g., O'Dea et al. 1988, Perley et al. 1982), and in marked contrast to the symmetric double-lobed morphologies commonly seen in extended steep-spectrum radio-loud QSOs (e.g., LBM93). The linear sizes of the core-dominated sources are significantly smaller: we measure a median value 7 kpc and maximum 60 kpc, which compares to 79 and 280 kpc for a subsample of 35 steep-spectrum ($\alpha \gtrsim 0.5$) LBM93 quasars, defined as having $\log L_{\rm ext.} \geq 27.0$. The latter figure is dictated by the detection limit of extended emission associated with the core-dominated quasars. Considering the core fractions, expressed in the R_5-parameter, the samples obviously differ: we find median $\log R_5$ values of -0.055 and -1.28 for the flat- and steep-spectrum sample respectively. While the former range from 0.0 to -0.41, the latter range from -0.05 to -2.87 (core fraction 0.13%). The radio luminosities of the extended emission differ much less markedly: median values are $\log L_{\rm ext.} = 27.2$ and 27.7 for the flat- and steep-spectrum sample respectively. The former value is still two orders of magnitude in excess of the Fanaroff & Riley (1974) break luminosity. This confirms earlier findings by O'Dea et al. (1988), Murphy et al. (1993), and Kollgaard et al. (1990): on the basis of their extended emission, many core-dominated, flat-spectrum radio sources need to be classified as Fanaroff and Riley class II sources, provided the extended emission is isotropic. As for the seven unresolved sources from our sample, we cannot as yet exclude the FR II classification.

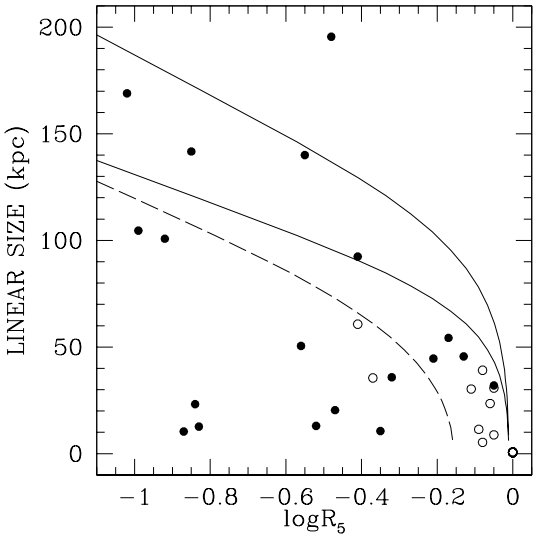

Fig. 1. Linear size vs. core fraction at 5 GHz for the combined sample of core- and lobe-dominated quasars, having $\log L_{\rm ext.} \geq 27.0$, and $-1 \leq \log R_5 \leq 0$. Open circles correspond to the observed flat spectrum quasars (Tables 1 and 3). The two solid lines describe the behaviour of a 500 kpc (350 kpc in lower curve) triple radio source with relativistic ($\gamma = 7.1$ or $\beta = .99$) nuclear jets giving rise to beamed core emission and foreshortened sizes at small inclination angles. The dashed curve describes the behaviour of a 350 kpc radio source with $\gamma = 4.1$ jets. The unbeamed core fraction was fixed by dictating $\log R_5(\theta = 45^\circ) = -2.5$. See text for details on data points and models.

Hence the major differences between the present flat-spectrum sample and the comparison sample of steep-spectrum quasars are the relative strengths of their radio cores and their morphological (a)symmetry and overall size. Variability data (e.g., factors of two on time scales of years) lead to brightness temperatures in excess of 10^{13}K, pointing towards beamed core emission (e.g., Kellermann & Pauliny-Toth 1981). To this

should be added the possible gamma-ray detection of 0458+020, most likely also signaling beamed radiation (e.g., Barthel et al. 1995). Therefore, rather than classifying the objects as intrinsically small sources, we prefer classification as normal extended double sources displaying beamed core emission and lobe foreshortening due to close alignment with the sight line of their radio axes.

Following Kapahi & Saikia (1982) we next investigate whether the linear sizes and core prominences support this view. Fig. 1 displays the linear size – $\log R_5$ behaviour for the present 16 sources, supplemented with 19 objects having $\log R_5$ in the range -1.0 to 0.0 – the interesting range for comparison – from the subsample of 35 LBM93 steep-spectrum quasars described above. The steep-spectrum objects are: 0225−014, 0238+100, 0352+123, 0445+097, 0751+298, 0758+120, 0805+046, 0941+261, 1023+067, 1055+499, 1354+258, 1402+044, 1540+180, 1554−203, 1607+183, 1701+379, 1726+344, 2223+210, and 2338+042. It should be noted that for these objects the R_5-values were evaluated using their measured spectral indices. It is clearly seen that high-R_5 objects commonly display extended emission. However, this emission does not exceed a few tens of kpc projected linear size. Low-R_5 objects display a considerably wider linear size range. The model lines describe the predicted behaviour of a triple (core plus two lobes) radio source with opposite relativistic nuclear jets, and intrinsic size L. With decreasing inclination angle, the effects of foreshortening and beamed core emission will increase, hence increasing $\log R_5$ with decreasing linear size in the model behaviour.

Defining θ as the angle between the radio source (jet) axis and the line of sight, a radio source having intrinsic linear size L, 5 GHz core fraction F_c and opposite jets with bulk flow speed $\beta = v/c$ will display a projected length

$$L(\theta) = L\ \sin(\theta)$$

as well as a core fraction (in the emitted frame)

$$R(\theta) = [2\,(1/F_c - 1)/B(\theta) + 1]^{-1}$$

where

$$B(\theta) = (1 - \beta\cos\theta)^{-2-\alpha} + (1 + \beta\cos\theta)^{-2-\alpha}$$

We adopt $\alpha = 0.8$ for the jet spectral index, and jet flow speed $\beta = 0.99$ (i.e., $\gamma = 7.1$) in evaluating the model, shown in Fig. 1, for intrinsic source sizes L of 350 and 500 kpc, respectively. Within current unification schemes (e.g., Barthel 1989) quasars are observed within jet inclination angles $\approx 45°$. LBM93 data show the largest quasars to have $\log R_5$ values ~ -2.5. On the basis of this finding the unbeamed core fraction $F_c \equiv R(\theta = 90°)$ was fixed by dictating $\log R_5(\theta = 45°) = -2.5$; this yields $\log F_c = -3.67$. In addition we computed the model behaviour for a $\gamma = 4.1$ ($\beta = 0.97$) $L = 350$ kpc radio source: this model is shown with the dashed line.

Similarly to Kapahi & Saikia (1982) and Saikia et al. (1991), it is seen that these relativistic jet models – obviously describing upper limits to linear size distributions – provide reasonable fits to the data. It is clear that for the assumed unbeamed core fraction $\log F_c = -3.67$ the $\gamma = 4.1$ model does not yield sufficient boosting to explain the high R_5 points, regardless of the inclination of the radio source. Hence, higher gamma factors and/or higher unbeamed core fractions must apply.

We conclude that $\log R_5$ is – on average – a good orientation indicator and that nuclear jet Lorentz factors $\approx$ 4–7 are likely. These findings are in broad agreement with results obtained for samples of (3CR) steep-spectrum quasars and radio galaxies by Bridle et al. (1994) and Fernini et al. (1997), with the latter authors measuring radio galaxy core fractions in the range $10^{-2.5}$ – $10^{-3.5}$. One caveat should however be mentioned, namely the possibility of the global radio source environment affecting the extended radio luminosity, and hence the R_5-parameter. In addition to core variability, some scatter in R may be attributed to these 'local weather' effects (cf. Wills & Brotherton 1995, Barthel & Arnaud 1996).

In order to avoid the contamination of a source intrinsic quantity with an environmental contribution, Wills & Brotherton (1995) proposed an improved measure of quasar orientation, R_V. As mentioned already in Sect. 2.4, this R_V parameter is defined as the ratio of the core radio luminosity at 5 GHz emitted frequency to the optical V-band luminosity, presumed to be AGN intrinsic quantities. Fig. 2 displays the linear size – $\log R_V$ behaviour for the combined sample of 16 flat and 19 steep-spectrum quasars. It is clear that only compact radio sources can display strong radio core dominance; large triple quasars display radio cores of considerably lower (V-band normalised) luminosity. Fig. 2 represents confirmation of the usefulness of $\log R_V$ as quasar orientation indicator, on the assumption that the upper envelope of the size distribution measures foreshortening proportional to the source inclination.

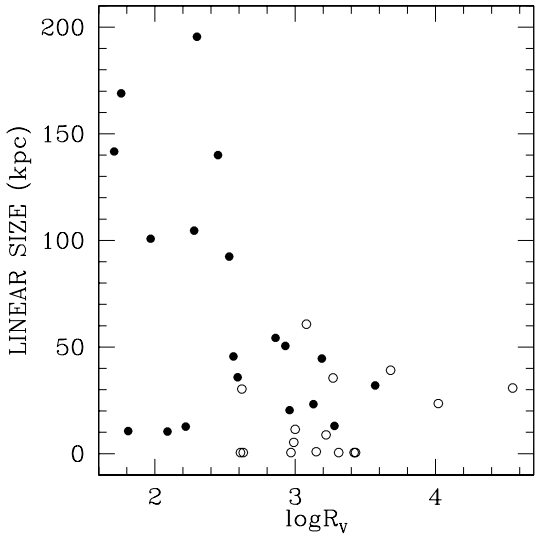

Fig. 2. Linear size vs. V-band luminosity normalized radio core luminosity (5 GHz) for the combined sample of 35 core- and lobe-dominated quasars from Fig. 1. See text for details on data points.

It should be stressed that the above analysis is very simplistic. Radio sources exist with a range in linear sizes, and a certain spread in F_c and γ must be present, as is evident from Fig. 1. Nevertheless, this and earlier analyses show that simplistic models provide agreement with the data, thereby providing support for the orientation scenario. Obtaining more data points for high R objects will be most valuable in assessing the magnitude of the beaming phenomena with more accuracy.

We have obtained optical spectra with the Palomar 200-inch telescope of 65 sample quasars (Barthel et al. 1990), and have enlarged this data base at the MMT (Vestergaard 1999). The purpose of this project is to combine radio and optical data, in a search for optical orientation indicators. The $\log R_5$ and $\log R_V$ parameters have here once again been shown to be useful orientation indicators, and we are therefore analyzing the optical spectra to search for parallel emission line orientation indicators. Radio-loud quasars offer the advantage that their orientation seems to be reflected in their Balmer line properties (e.g., Wills & Browne 1986). We attempt to find similar orientation indicators in the ultraviolet part of the spectrum, which can be used to address the orientation of high redshift QSOs in general. In addition, we plan to carry out a detailed comparison of quasar emission line parameters, for radio-loud, radio-quiet, and radio-silent QSOs, in search for radio-loudness indicators and radio morphological correlations. Earlier attempts (e.g., Corbin & Francis 1994) suffer from unreliable radio spectral information and the lack of radio maps. The results of our investigations will be communicated in forthcoming publications.

Acknowledgements. We acknowledge the excellent APM facility, CCD imaging by Rien Dijkstra, and comments on the manuscript by Belinda Wilkes and the referee Dr. G.B. Taylor. PDB acknowledges travel support from the Leids Kerkhoven-Bosscha Fonds. MV is very pleased to thank the Smithsonian Astrophysical Observatory and the High Energy Division for their hospitality. MV also gratefully acknowledges financial support from the Danish Natural Sciences Research Council (SNF-9300575), the Danish Research Academy (DFA-S930201) and a Research Assistantship at Smithsonian Astrophysical Observatory made possible through NASA grants (NAGW-4266, NAGW-3134, NAG5-4089; P.I.: Belinda Wilkes). The NRAO VLA is a facility of the National Science Foundation operated under cooperative agreement by Associated Universities, Inc. This research has made use of the NASA/IPAC Extragalactic database (NED) which is operated by the Jet Propulsion Laboratory, Caltech, under contract with the National Aeronautics and Space Administration.

Appendix A:

Figs. 3–11 are VLA images at 5 GHz of 9 core-dominated quasars, with resolving beams shown in each image. The contour levels, expressed as multiples of the approximate 1σ image noise level as well as the image peak flux density are specified under each image. These numbers are also specified in Table 2. With reference to Table 1, crosses mark the optical QSO positions with their associated uncertainties.

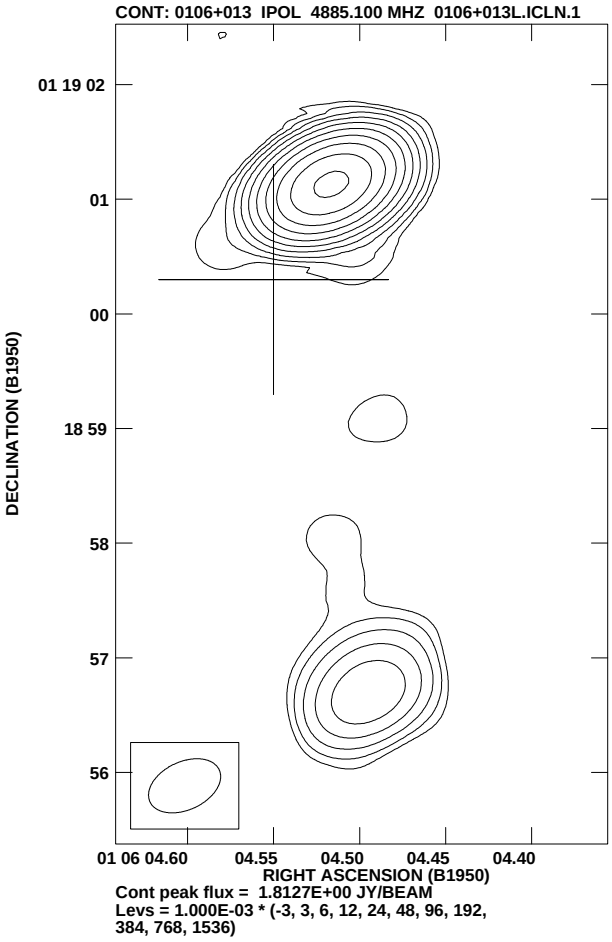

Fig. 3.

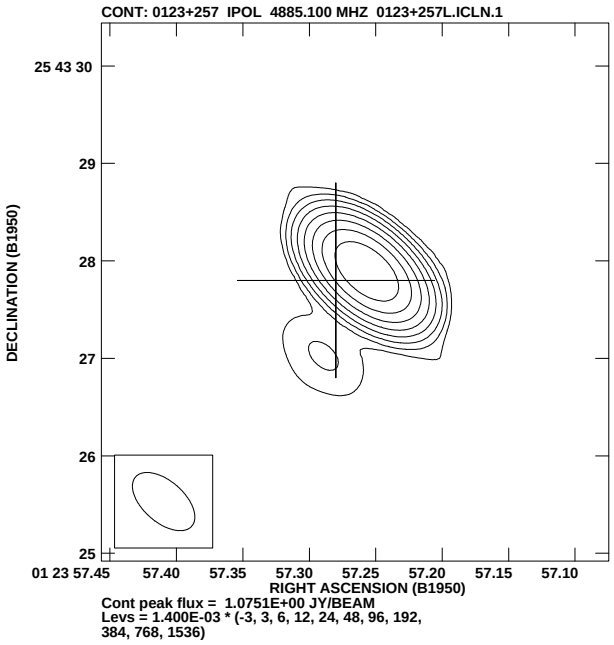

Fig. 4.

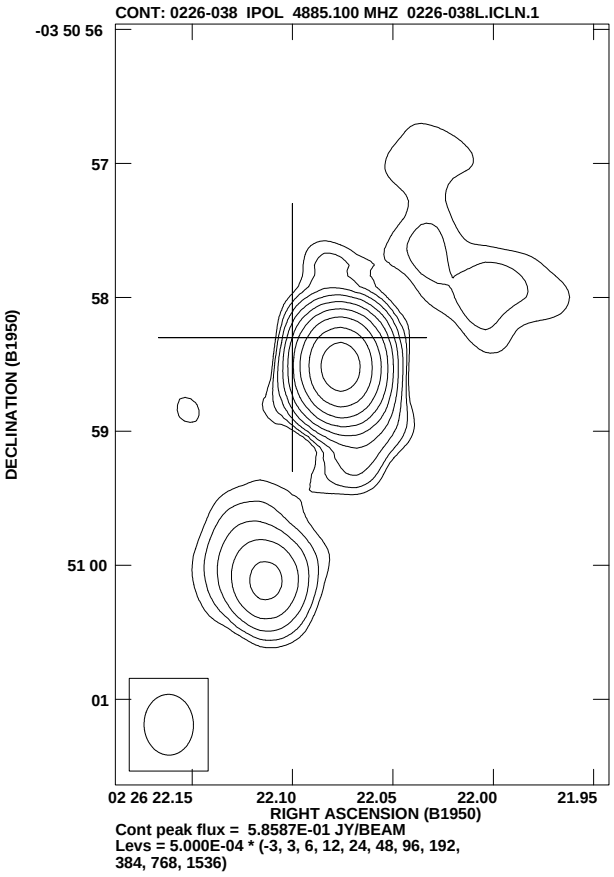

Fig. 5.

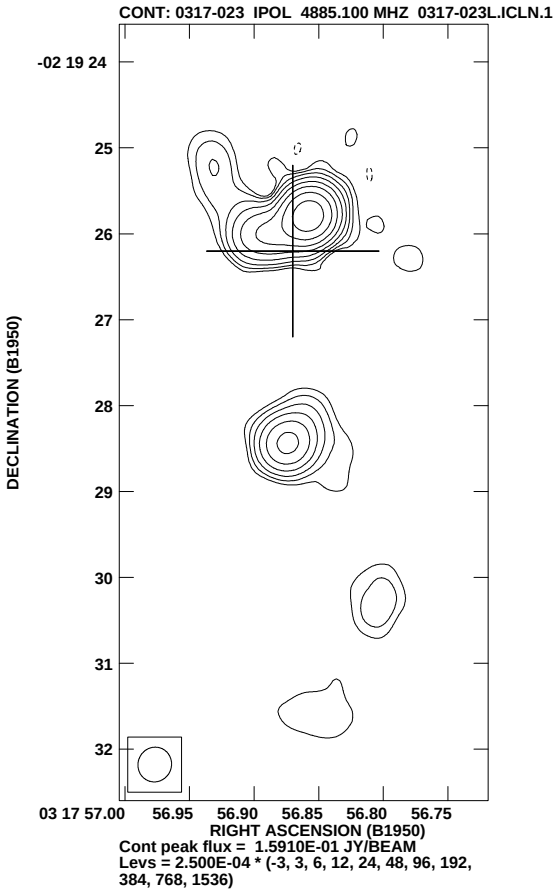

Fig. 6.

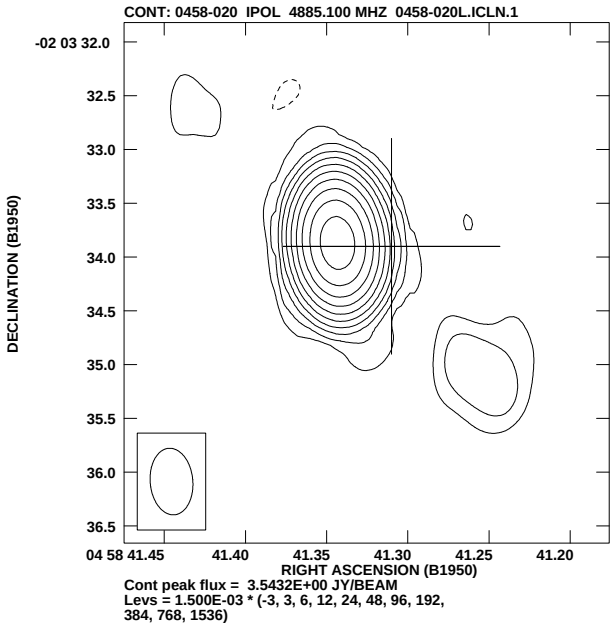

Fig. 7.

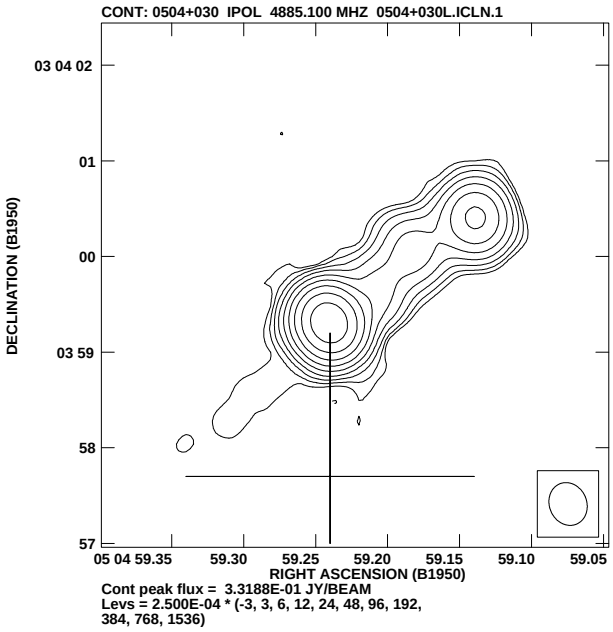

Fig. 8.

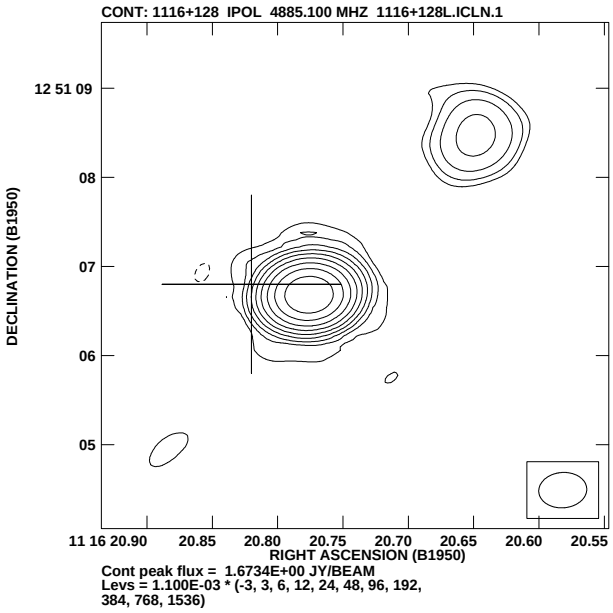

Fig. 9.

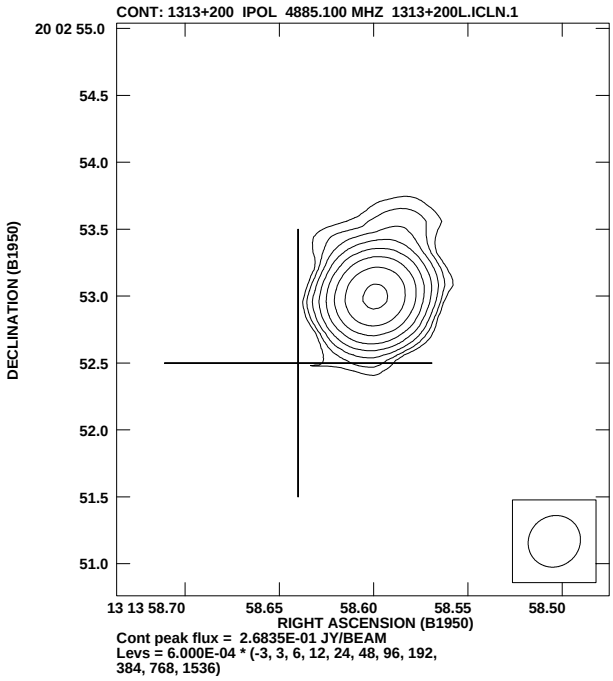

Fig. 10.

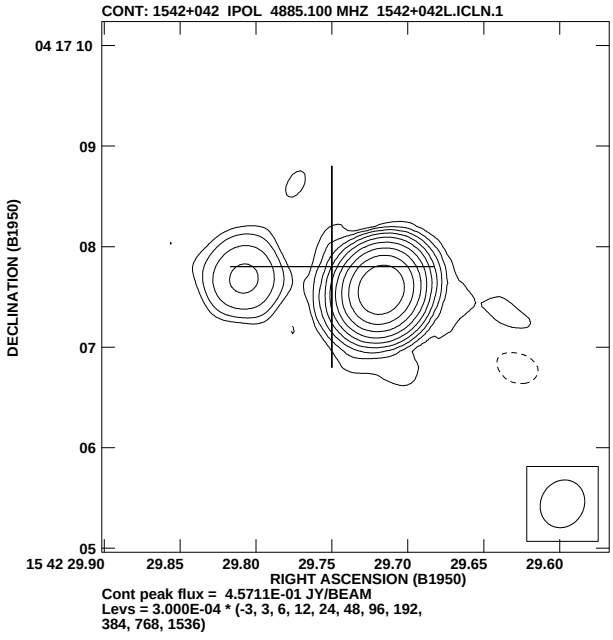

Fig. 11.

References

Barthel P.D., 1989, ApJ 336, 606
Barthel P.D., Arnaud K.A., 1996, MNRAS 283, L45
Barthel P.D., Tytler D.R., Thomson B., 1990, A&AS 82, 339
Barthel P.D., Conway J.E., Myers S.T., et al., 1995, ApJ 444, L21
Becker R.H., White R.L., Edwards A.L., 1991, ApJS 75, 1 (B91)
Bolton J.G., Shimmins A.J., Wall J.V., 1975, Aust. J. Phys. Astrophys. Suppl. 34, 1
Bridle A.H., Hough D.H., Lonsdale C.J., et al., 1994, AJ 108, 766
Corbin M.R., Francis P.J., 1994, AJ 108, 2016
De Vries W.H., O'Dea C.P., Baum S.A., et al., 1998, ApJ 503, 156
Fanaroff B.L., Riley J.M., 1974, MNRAS 167, 31P
Fanti R., Fanti C., Schilizzi R.T., et al., 1990, A&A 231, 333
Fernini I., Burns J.O., Perley R.A., 1997, AJ 114, 2292
Griffith M.R., Wright A.E., Burke B.F., Ekers R.D., 1995, ApJS 97, 347 (G95)
Hewitt A., Burbidge G., 1993, ApJS 87, 451
Kapahi V.K., Saikia D.J., 1982, JA&A 3, 465
Kellermann K.I., Pauliny-Toth I.I.K., 1981, ARA&A 19, 373
Kollgaard R.I., Wardle J.F.C., Roberts D.H., 1990, AJ 100, 1057
Kühr H., Witzel A., Pauliny-Toth I.I.K., Nauber U., 1981, A&AS 45, 367
Lonsdale C.J., Barthel P.D., Miley G.K., 1993, ApJS 87, 63 (LBM93)
Murphy D.W., Browne I.W.A., Perley R.A., 1993, MNRAS 264, 298
O'Dea C.P., 1998, PASP 110, 493
O'Dea C.P., Barvainis R., Challis P.M., 1988, AJ 96, 435
Orr M.J.L., Browne I.W.A., 1982, MNRAS 200, 1067
Perley R.A., Fomalont E.B., Johnston K.J., 1982, ApJ 255, L93
Punsly B., 1995, AJ 109, 1555
Readhead A.C.S., Taylor G.B., Pearson T.J., Wilkinson P.N. 1996, ApJ 460, 634
Saikia D.J., Singal A.K., Wiita P.J., 1991, In: Miller H.R., Wiita P.J. (CUP) (eds.) Variability of active galactic nuclei. p. 160
Shimmins A.J., Bolton J.G., Wall J.V., 1975, Aust. J. Phys. Astrophys. Suppl. 34, 63
Thompson D.J., Bertsch D.L., Dingus B.L., et al., 1995, ApJS 101, 259
Udomprasert P.S., Taylor G.B., Pearson T.J., Roberts D.H., 1997, ApJ 483, L9
Urry C.M., Padovani P., 1995, PASP 107 803
Véron-Cetty M.-P., Véron P., 1987, A Catalogue of Quasars and Active Nuclei. ESO Scientific Report No. 5
Vestergaard M., 1999, Ph.D. Thesis, University of Copenhagen
Wall J.V., 1972, Aust. J. Phys. Astrophys. Suppl. 24
Wall J.V., Bolton J.G., Wright A.E., et al., 1976, Aust. J. Phys. Astrophys. Suppl. 39
Wills B.J., Brotherton M.S., 1995, ApJ 448, L81
Wills B.J., Browne I.W.A., 1986, ApJ 302, 56
Wills B.J., Wills D., 1979, ApJS 41, 689